

## Article

# Anomaly Detection in Spatiotemporal Data from Fiber Optic Distributed Temperature Sensing for Outdoor Fire Monitoring

Haitao Bian <sup>1,2</sup>, Xiaohan Luo <sup>1</sup>, Zhichao Zhu <sup>1</sup>, Xiaowei Zang <sup>1,2,\*</sup> and Yu Tian <sup>1</sup>

<sup>1</sup> College of Safety Science and Engineering, Nanjing Tech University, Nanjing 211816, China; bianhaitao@njtech.edu.cn (H.B.)

<sup>2</sup> Jiangsu Key Laboratory of Hazardous Chemicals Safety and Control, Nanjing Tech University, Nanjing 211816, China

\* Correspondence: nanozang@njtech.edu.cn

**Abstract:** Outdoor fire detection faces significant challenges due to complex and variable environmental conditions. Fiber Optic Distributed Temperature Sensing (FO-DTS), recognized for its high sensitivity and broad monitoring range, provides significant advantages in detecting outdoor fires. However, prediction models trained in laboratory settings often yield false and missed alarms when deployed in complex outdoor settings, due to environmental interferences. To address this issue, this study developed a fixed-power fire source simulation device to establish a reliable small-scale experimental platform incorporating various environmental influences for generating anomalous temperature data. We employed deep learning autoencoders (AEs) to integrate spatiotemporal data, aiming to minimize the impact of outdoor conditions on detection performance. This research focused on analyzing how environmental temperature changes and rapid fluctuations affected detection capabilities, evaluating metrics such as detection accuracy and delay. Results showed that, compared to AE and VAE models handling spatial or temporal data, the CNN-AE demonstrated superior anomaly detection performance and strong robustness when applied to spatiotemporal data. Furthermore, the findings emphasize that environmental factors such as extreme temperatures and rapid temperature fluctuations can affect detection outcomes, increasing the likelihood of false alarms. This research underscores the potential of utilizing FO-DTS spatiotemporal data with CNN-AE for outdoor fire detection in complex scenarios and provides suggestions for mitigating environmental interference in practical applications.

**Keywords:** outdoor fire detection; anomaly temperature detection; fiber optic distributed temperature sensing; spatiotemporal data; environmental interferences



Academic Editor: Jiajian Zhu

Received: 28 November 2024

Revised: 7 January 2025

Accepted: 8 January 2025

Published: 10 January 2025

**Citation:** Bian, H.; Luo, X.; Zhu, Z.; Zang, X.; Tian, Y. Anomaly Detection in Spatiotemporal Data from Fiber Optic Distributed Temperature Sensing for Outdoor Fire Monitoring. *Fire* **2025**, *8*, 23. <https://doi.org/10.3390/fire8010023>

**Copyright:** © 2025 by the authors. Licensee MDPI, Basel, Switzerland. This article is an open access article distributed under the terms and conditions of the Creative Commons Attribution (CC BY) license (<https://creativecommons.org/licenses/by/4.0/>).

## 1. Introduction

Outdoor fires are a common and destructive type of disaster worldwide, causing significant damage to ecosystems, human lives, and economic activities. Typical scenarios of outdoor fires include exterior buildings [1], electrical equipment [2], forests [3], grassland [4], and industrial facilities [5,6]. Large areas of forest and grassland are affected by wildfires annually, severely disrupting ecological balance and posing significant threats to human safety and property. Therefore, timely and effective outdoor fire warnings are crucial for minimizing property loss and protecting the environment [7–14].

Abnormal temperature detection, as an effective early fire-warning mechanism, achieves precise temperature monitoring and provides alerts through the use of various

sensors and anomaly detection algorithms. Commonly used sensors include thermocouples, thermistors, infrared sensors, and infrared thermal cameras, all of which provide high-precision temperature measurements in diverse environments [15]. Researchers have developed a variety of anomaly detection methods to analyze sensor data and identify abnormal patterns that deviate from normal temperature fluctuations. A survey report conducted a comprehensive and systematic review of anomaly detection methods across almost two decades, covering approaches based on density, statistics, distance, clustering, ensemble algorithms, and machine learning [16]. These algorithms analyze temperature data collected by sensors to identify abnormal patterns deviating from normal states and trigger warning signals. Among these methods, machine learning techniques, known for their powerful feature extraction and pattern recognition capabilities, have proven particularly effective in handling complex and nonlinear temperature data, gradually becoming the dominant approach [17,18], significantly enhancing the accuracy and responsiveness of anomaly detection [19].

However, compared with indoor fires, outdoor fires present significant complexity and challenges. Outdoor fires tend to be more dispersed and spread more rapidly, heavily influenced by various environmental factors such as temperature, humidity, wind speed, and weather conditions [20,21]. The accuracy and sensitivity of abnormal temperature detection systems in practical applications are often affected by these environmental factors. For instance, natural conditions such as ambient temperature, humidity, wind speed, and weather can substantially impact the actual measurement of abnormal temperature rises [22–24]. These factors may cause temperature readings from sensors to inaccurately reflect abnormal heating events, as they are influenced by environmental interference. Such interference affects changes in data patterns and the extraction of abnormal features, causing detection models designed under laboratory conditions to deviate when used in practical applications. Because the temperature data fed into the model are impacted by environmental factors, this can lead to false negatives or false positives in fire warning systems [25].

Specifically, in fire detection for outdoor scenarios, such as forests, grassland, and outdoor equipment, high-temperature and high-humidity environments reduce thermal diffusion capacity, leading to more intense temperature rises and an increased fire risk. Conversely, under low-temperature and low-humidity conditions, rapid heat dissipation may obscure abnormal temperature increases during the early stages of a fire, resulting in delayed warnings. When wind speeds are high, temperature variations at the fire source become more dispersed and less concentrated, increasing the difficulty of detecting abnormal temperatures. Rainfall and snowfall can quickly lower the surface temperatures of the ground and equipment, concealing early signs of abnormal heating. Additionally, shifts in the monitored area between direct sunlight and shadow cause significant temperature fluctuations, masking the true temperature distribution and hindering the timely identification of early signs of abnormal heating indicative of fire events [26,27].

To mitigate the impact of environmental factors on abnormal temperature detection systems, researchers have proposed various improvement methods. Researchers have employed empirical correction methods, adjusting temperature monitoring thresholds based on prior experience and historical data analysis [28]. However, these methods are highly subjective with limited applicability and reliability in different environments. With advancements in machine learning, researchers have attempted to address these issues by improving data-driven models through improving their robustness to environmental factors and introducing composite data approaches [29,30]. In this study, the composite data were the spatiotemporal temperature datasets collected during outdoor fire simulations, capturing temperature variations across different times and spatial locations. This dataset

reflected dynamic changes in monitored temperatures over time and space, offering a more comprehensive perspective for the model and enabling more accurate identification of abnormal temperature variations for fire warnings. By integrating both temporal and spatial data into the model's input, the spatiotemporal characteristics of the data are fully utilized, enhancing the model's performance and reducing false alarms and missed detection caused by environmental temperature fluctuations.

In this context, FO-DTS offers a promising solution to improve the reliability and accuracy of outdoor fire detection. Unlike traditional point sensors such as thermocouples and early single-point fiber optic sensors (e.g., fiber Bragg gratings), FO-DTSs provide continuous temperature distribution along the fiber, with measurement distances ranging from tens of meters to tens of kilometers. This makes FO-DTSs highly suitable for fire monitoring in large areas such as storage tanks, construction sites, forests, and grasslands [31]. The measurement process of an FO-DTS is based on optical scattering, making it immune to electromagnetic interference, which is ideal for use in harsh field environments, ensuring stability and reliability in complex surroundings [32]. Moreover, FO-DTS offers more flexible deployment, which enhances their suitability for various fire monitoring applications.

Integrating emerging sensor technologies and data-driven algorithms is crucial for developing reliable systems for abnormal temperature detection. The application of emerging sensor technologies provides more comprehensive temperature data at anomaly detection sites, leading to more accurate and reliable results. Simultaneously, data-driven methods, particularly deep learning techniques such as autoencoders (AEs), have achieved notable success in anomaly detection [33]. An AE is a neural network model used for unsupervised feature extraction. It learns compressed representations of the data to reconstruct the input data. An AE consists of two parts: an encoder that maps the input data to a compressed latent space, and a decoder that reconstructs the original input from the latent representation. During training, the AE aims to minimize the reconstruction errors between the input and the output, effectively capturing the underlying structure of the data [34,35]. When used for anomaly detection, the AE model is first trained on normal data to learn the normal patterns. Subsequently, for new data, if the reconstruction errors exceed a predefined threshold, the data point is considered anomalous. This approach is particularly effective for anomaly detection in complex, high-dimensional data, as traditional methods may perform poorly in such cases due to issues like data imbalance, high dimensionality, or the lack of labeled data [36–38]. This study proposes an AE-based method for detection of anomalous temperatures in spatiotemporal fiber optic distributed temperature sensor data, aiming to achieve early warning for incidents such as fires. This method improves the accuracy of the anomaly temperature detection system in the presence of environmental factors by integrating spatial and temporal dimensions, thereby reducing the risks of false alarms and missed detection.

This paper explores the effectiveness of an AE model that integrates two-dimensional spatiotemporal data for anomaly temperature detection, considering the specific characteristics of FO-DTS and the challenges posed by environmental factors. The objective is to achieve accurate detection of temperature anomalies in outdoor fire warning systems and mitigate the risks of false alarms and missed detections and investigate the environmental influences in the detection process. The structure of this paper is as follows. Section 2 introduces the methodology for detection of temperature anomalies and the experimental equipment setup. Section 3 presents the results and discussions from the perspectives of temporal, spatial, and spatiotemporal analysis. Section 4 concludes this study and outlines future research directions.

## 2. Methodology

The proposed system architecture is shown in Figure 1. The public meteorological information server provides weather information to the embedded system gateway via Ethernet. Temperature and humidity sensors send on-site temperature and humidity data to the embedded system gateway through the Modbus protocol. Then, the AT800 FO-DTS (Suzhou Agioe Technologies Co., Ltd., Suzhou, China) collects temperature data and forwards these to the embedded system gateway via the MQTT protocol. Subsequently, the embedded system gateway processes these data and stores them in the local MySQL database (Community Edition 8.0). Finally, the system employs AE models for anomaly detection, ensuring any abnormal conditions can be promptly identified. The AE models were implemented using PyTorch 1.12.1 with CUDA 11.6 for GPU acceleration on Ubuntu 22.04, and the python version is 3.9.

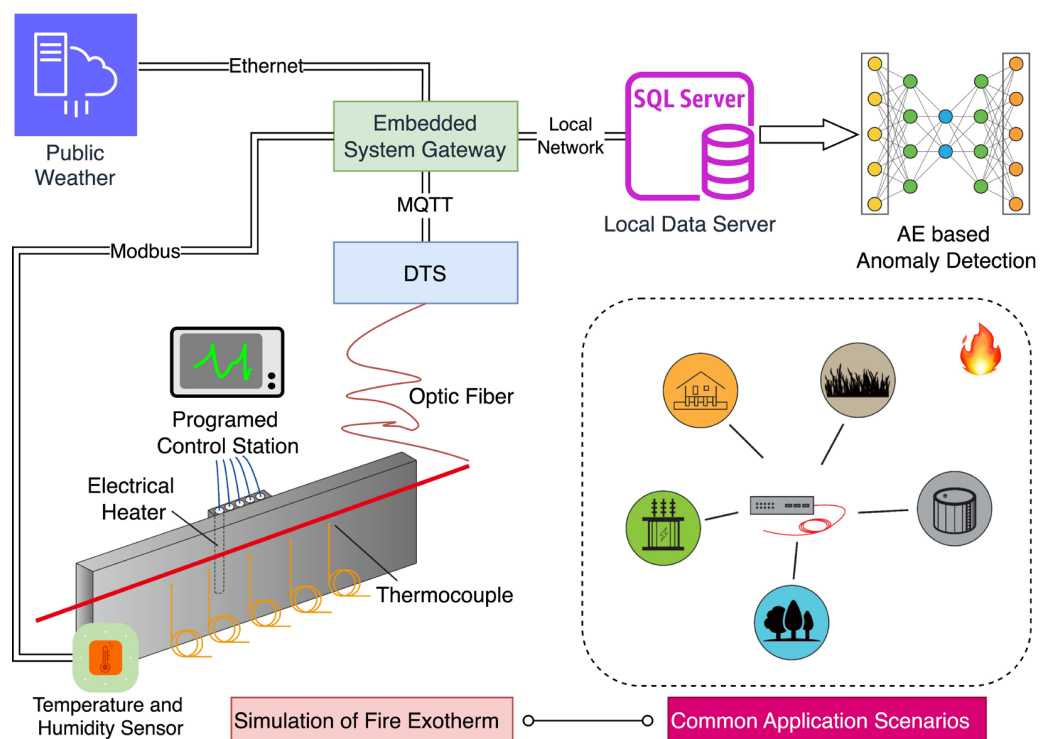


**Figure 1.** Architecture for anomalous temperature detection for outdoor fire warning systems.

### 2.1. Experiment

In the context of the time-consuming nature of outdoor fire experiments and safety hazards associated with using real fire sources, a constant power heating device can provide safe, controllable, and repeatable experimental conditions and accurately simulate the temperature change characteristics in the early stages of a fire [39]. Therefore, a constant-power electric heating module was used to heat a steel plate, simulating the rapid temperature rise process in the early stages of a fire. As shown in Figure 1, an experimental setup was designed to simulate the scenario of using an FO-DTS for abnormal temperature detection in an outdoor fire warning system, and to obtain temperature measurements under both normal and abnormal conditions. Outdoors, a constant-power fire-source simulation device plate was used to simulate the outdoor fire, with dimensions of 1200 mm × 345 mm × 15 mm. A customized heating module (100 mm × 100 mm) was installed on the back of the test plate. Five electrical heating rods (120 W) were embedded in the heating module, and a solid-state relay drive controlled the heating power with pulse width modulation generated from an embedded system. Five thermocouples were arranged on

the front of the steel plate at 100 mm intervals, and the optical fiber was placed 5 mm away from the surface of the plate. Near this apparatus, temperature and humidity sensors were installed to record local environmental information. A thermocouple is a traditional point temperature sensor with very high accuracy and speed of response. It can accurately measure the temperature at a specific point without being limited by spatial resolution. Compared with thermocouples, the measurement results of an FO-DTS are far from the actual situation due to the spatial resolution, and it is difficult to distinguish the anomalies intuitively. Therefore, in this experiment, the main role of the thermocouple was to provide intuitive anomaly detection results.

The FO-DTS used in this experiment was based on Raman scattering and optical time-domain reflection. The spatial resolution of the FO-DTS was 500 mm and the precision of temperature measurement was 0.1 °C. The FO-DTS returned a temperature value every 100 mm along the fiber at intervals of 3 s. The thermocouples returned data every 3 s; since both had the same time sampling interval (both 3 s), it was easy to compare temperature data for the same moment. The other sensors were set to 30 s. All the above information was collected and saved in a local database.

The experiments were conducted outdoors in the summer in Nanjing, China. The experimental platform was fixed in an east-facing position so that it would be exposed to sunlight in the morning and hidden in the shade in the afternoon. Normal data were collected when the heating device was not working, and five different anomalous scenarios were created by heating the plate under different environmental conditions (all with a heating power of 120 W). The five scenarios covered morning, noon, afternoon, and evening, with temperatures ranging from 30.3 °C to 45.4 °C and humidity ranging from 32% to 81.6%, including both sunny and cloudy weather conditions. The patterns of temperature anomalies for the different scenarios are also shown in Figure 2. The environmental information for the different scenarios is presented in Table 1, where the time in the table indicates the time of the start of the experiment, i.e., the exact moment when the heating unit started working.

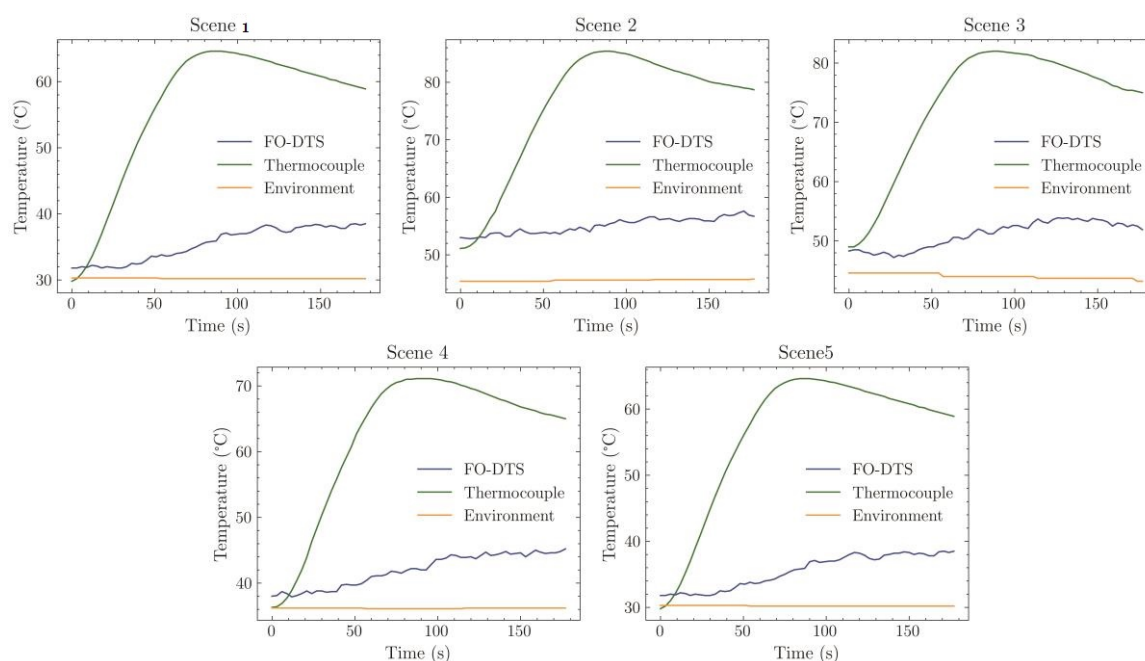


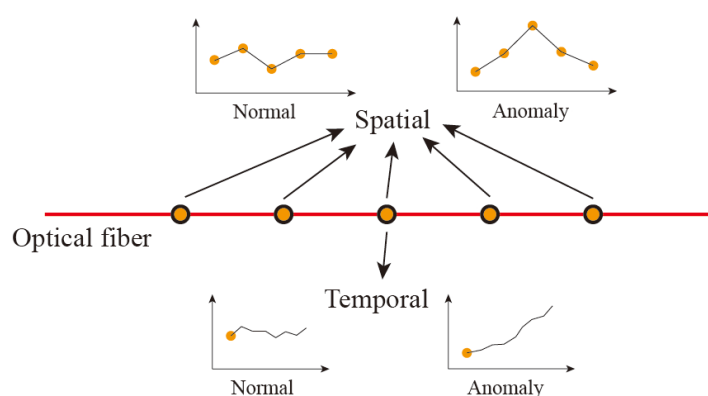
**Figure 2.** Abnormal temperature changes in different environmental scenarios.

**Table 1.** The details of the ambient information in anomaly scenes.

Scenes	Time	Temperature (°C)	Humidity (%)	Weather
1	12:16	37.9	54	Cloudy
2	9:27	45.4	32	Sunny
3	10:24	44.6	34.2	Sunny
4	15:04	36.2	57	Sunny
5	21:48	30.3	81.6	Cloudy

## 2.2. Detection of Temperature Anomalies via FO-DTS

Different from other temperature sensors, an FO-DTS offers both spatial and temporal information. Consequently, when an anomaly occurs, the collected field data can be analyzed from two perspectives, as illustrated in Figure 3, where the orange dots represent continuous measurement points along the FO-DTS sensing optical fiber.

**Figure 3.** Two perspectives for detecting anomalous temperatures via FO-DTS.

From the spatial perspective, due to the existence of spatial resolution, the system may not precisely match the actual temperatures at certain scales. When detecting a relatively small hotspot, several continuous points along the FO-DTS record the temperature, with points closer to the hotspot typically registering higher temperatures. However, if a hotspot extends beyond the spatial resolution of the system, the FO-DTS can accurately report the temperature according to the thermocouple. Thus, for anomaly detection from the spatial perspective, the continuous temperature at a particular time can be used to either estimate the hotspot temperature or evaluate the system state. The environmental conditions at different positions within a small range of fiber are uniform; therefore, the temperature from continuous measurement points changes synchronously under environmental influence. Anomalies in temperature at a specific location cause spatial variations in the measured values, which is fundamental to detecting anomalous temperatures from the spatial perspective.

From the temporal perspective, temperature variations at a specific location are influenced by environmental effects. Distinguishing the characteristics of temperature changes under normal conditions from those under anomalous conditions enables effective detection of anomalies. However, environmental fluctuations often complicate this distinction, leading to potential false alarms. For instance, minimal measurement fluctuations pose significant challenges in detecting temperature anomalies, necessitating the use of algorithms to enhance detection accuracy.

## 2.3. Detection of Anomalous Temperatures with AE

The imbalance between normal data (i.e., data collected when no fire occurs) and abnormal data (i.e., data collected during a fire) presents challenges for traditional supervised

learning methods. Traditional models may overfit the normal data, thereby weakening their ability to detect abnormal data [40,41]. In contrast, as an unsupervised learning method, AEs are particularly well suited for scenarios with data imbalance because they do not require a large amount of abnormal data for training. An AE can be trained with only normal data, learning to reconstruct normal patterns. For new data, if the reconstruction errors exceed a set threshold, the data point is considered anomalous [36]. Moreover, the temperature data obtained using the FO-DTS contains both spatial and temporal dimensions, with many measurement points and timestamps for each dimension. Traditional methods may perform poorly in this context due to the curse of dimensionality or the lack of labeled data. In contrast, an AE can effectively capture the underlying structure of high-dimensional data by learning compressed representations, thereby improving the accuracy of anomaly detection. Therefore, these characteristics make AEs an ideal choice for handling imbalanced, high-dimensional temperature data.

Specifically, an AE is a data reconstruction model consisting of an encoder and a decoder. The original data  $X$  are first passed through the encoder, which extracts their features ( $f : X \rightarrow F$ ). The extracted information is then delivered into the decoder to attempt to restore the original data ( $g : F \rightarrow \hat{X}$ ). The loss between output  $\hat{X}$  and input  $X$  is used to optimize the algorithm, enabling it to capture the input features and generate an output that closely resembles the original data (Equation (1)).

$$f, g = \arg \min_{f, g} \|X - g[f(X)]\|^2 \quad (1)$$

The convolutional autoencoder (CNN-AE) replaces the fully connected layers of a traditional autoencoder with convolutional layers, enabling it to more effectively handle input data with spatial structures. For the input  $a$ , linear layers process the data via linear calculation, as  $z = W^T a + b$ , where  $w$  and  $b$  are weight vector and bias. For convolution layers, the input is processed by cross-correlation, as  $z = K \otimes a + b$ , where  $K$  is the kernel. The cross-correlation can be described via Equation (2):

$$y_{i,j} = \sum_{u=1}^U \sum_{v=1}^V K_{u,v} X_{i+u-1, j+v-1}, K \in R^{U \times V} \quad (2)$$

The VAE operates as an encoding–decoding framework that utilizes variational inference to model the probability distribution of the input data by approximating it with a simpler distribution family. The VAE's encoder outputs the approximate posterior distribution of the latent variable  $z$ , which can be described as  $q(z|x; \phi)$ , and the decoder is the likelihood of input  $x$ , which is  $p(x|z; \theta)$ . For simplicity,  $q(z|x; \phi)$  is commonly postulated as Gaussian distribution, so the latent variable  $z$  or the outputs of encoder are mean  $\mu$  and variance  $\sigma^2$ . To ensure  $z$  had independent randomness, a reparameterization trick expressed via Equation (3) was applied:

$$z = \mu + \sigma \odot \epsilon, \epsilon \sim \mathcal{N}(0, I) \quad (3)$$

In the detection of temperature anomalies, normal data are sent for training the AE, and the algorithm can learn the features of the normal conditions. When an anomaly occurs, the AE, unfamiliar with the anomaly's features, generates a larger loss between the output and the input. If this loss exceeds a predefined threshold, an anomaly is detected. Normal data are split into training and test sets. The threshold is commonly set as a certain percentile of this loss array or according to kernel density estimation corresponding to a certain confidence level. Consequently, the threshold setting is somewhat subjective and adjustable, affecting the sensitivity of anomaly detection. To compare different conditions equally, a test set is used to balance the performance. After a default threshold is determined, it is

used for detection within the test set, which includes the datasets of temperature anomalies simulated by electrical heating. The results can be used to evaluate the performance of the algorithms. Due to the ambiguous boundary between normal and anomalous states, the loss from anomalies may fall below the set threshold, while loss from the normal state may exceed it. Algorithms that more accurately extract normal features are often better at identifying anomalies and can more quickly return anomaly results. In this study, the delay in temperature anomaly detection—defined as the time taken for the algorithm to return anomaly results after heating began—served as a key metric for evaluating the detection performance.

In this study, we conducted anomaly detection from temporal, spatial, and spatiotemporal perspectives using various AE models. The workflow for this process is shown in Figure 4. To ensure that the data accurately reflected temperature variations during the occurrence and development of the fire, we employed a rigorous data selection strategy.

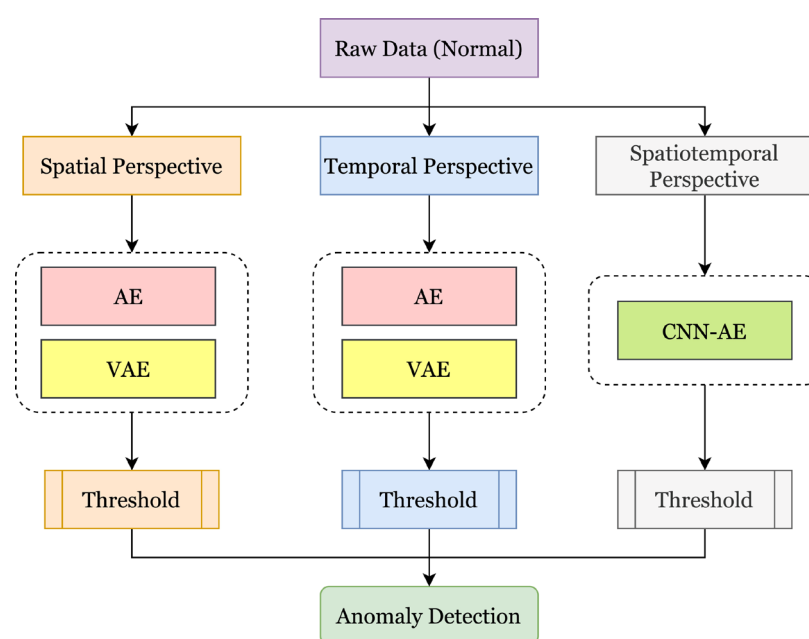


**Figure 4.** The workflow of temperature anomaly detection in this study.

### 2.3.1. Temporal Perspective Anomaly Detection

Time series data are one of the most commonly used types of data used in current research, widely applied in fields such as anomaly detection, forecasting, and pattern recognition [42]. In this study, within the time series dimension, we selected the temperature data of all timestamps from the measurement point at the middle position of the experimental board’s FO-DTS. This point was located at the heating source and represented the most significant temperature change. By focusing on a fixed spatial point, the influence of spatial variables on time series features can be minimized. Then, a sliding window technique was used to capture the dynamic features of the time series data, where each sliding window contained temperature values from multiple consecutive time points. The data from these sliding windows were proportionally divided into training and test sets.

For anomaly detection in time series data, this study used an AE and a VAE. First, the temperature data from all timestamps at the middle measurement point were used as input to form sliding window sequences. Then, the AE and VAE models were trained using time series data from normal conditions. The AE model learned the normal patterns by minimizing the reconstruction errors between the input and output, while the VAE model introduced a probabilistic generative model and was trained by maximizing the

log likelihood of the data. During training, the AE and VAE models both learned to extract features from the normal data and reconstruct the input data. For new data, the reconstruction errors (AE) or reconstruction loss (VAE) was calculated. If the reconstruction errors or loss exceeded a predefined threshold, the data point was considered anomalous. The 95th percentile of the reconstruction errors from the training set was selected as the threshold to ensure a low false-positive rate.

### 2.3.2. Spatial Perspective Anomaly Detection

In the spatial dimension, we selected all measurement points along the entire monitoring path of the FO-DTS. Each ID represented the temperature measurement points at different spatial locations at the same time, with each ID corresponding to 10 temperature feature points. In the early stages of a fire, temperature increases are often confined to a specific area. The collection of multi-point spatial data can significantly enhance the sensitivity and reliability of fire detection systems. Temperature differences across different locations can be substantial, with higher temperatures closer to the heating source and lower temperatures further away. This difference can affect the model's learning process, causing temperature data from certain locations to be either overemphasized or overlooked. Therefore, we normalized the temperature data collected along the FO-DTS path to eliminate dimensional differences and ensure that all data were compared and processed on the same scale. For each ID corresponding to 10 temperature points, we extracted spatial features by calculating statistics such as the difference, mean, and standard deviation between adjacent temperature points to enhance the AE model's ability to capture local anomalies.

For the spatial dimension data, this study used an AE and a VAE for anomaly detection. First, the temperature data from all measurement points along the FO-DTS monitoring path were used as input, forming multiple spatial vectors, each containing 10 features. The data from all IDs together formed a complete spatial feature matrix. The AE and VAE models were trained using the spatial data under normal conditions. The AE model learned the normal spatial temperature distribution by minimizing the reconstruction errors between the input and output, while the VAE introduced a probabilistic generative model and was trained by maximizing the log likelihood of the data. During training, the AE and VAE models both learned to extract features from the normal data and reconstruct the input data. For new data, the reconstruction errors (AE) or reconstruction loss (VAE) for the spatial vector corresponding to each ID was calculated. If the reconstruction errors or loss for a particular ID exceeded the predefined threshold, it was considered that an anomaly existed at that location. The 95th percentile of the reconstruction errors from the training set was selected as the threshold to ensure a low false-positive rate.

### 2.3.3. Spatiotemporal Perspective Anomaly Detection

To comprehensively consider both the temporal and spatial dimensions and fully capture the temperature changes during the occurrence and development of a fire, this study combined the spatial data from all measurement points along the entire monitoring path with the time series data captured using the sliding window technique, forming a spatiotemporal dataset containing both temporal and spatial information. For each timestamp, the temperature data from all measurement points were combined into a spatial vector containing 10 features. Each spatial vector represented the temperature values at 10 different locations for that timestamp. For each sliding window, spatial vectors from multiple timestamps were stacked together, forming a 2D sample with the shape [window length, spatial feature number]. These samples were proportionally divided into training and test sets.

For the spatiotemporal data, we used a convolutional autoencoder (CNN-AE) for anomaly detection. The collected samples used as model input contains both temporal and spatial information. The CNN-AE model was trained using spatiotemporal data under normal conditions. The encoder part extracted local features through multiple convolutional layers, while the decoder part reconstructed the input data using deconvolution layers, with the goal of minimizing the reconstruction errors between the input and output. Fully connected layers were added between the encoder and decoder to further compress and expand the features, ensuring that the model was able to learn higher-level abstract representations. During training, the mean squared error (MSE) was used as the loss function, and model parameters were optimized through the backpropagation algorithm. The 95th percentile of the reconstruction errors from the training set was selected as the threshold. For new data, the reconstruction errors were calculated. If the reconstruction error exceeded the predefined threshold, the data point was considered anomalous.

### 3. Results and Discussion

#### 3.1. Detection of Anomalous Temperatures from the Temporal Perspective

##### 3.1.1. Temporal Model Design and Setting

To capture the spatiotemporal properties in the time series data, we employed a sliding window technique, where each window contained temperature values from multiple time points. Temperature values returned from measurement point 5 in the middle of the FO-DTS were chronologically programmed into a sliding window to ensure that the model captured the characteristics of temperature changes over short periods of time. The input lengths of temperature sequences were 10, representing a 30-s interval, totaling 303,911 samples after division of normal data. All normal data were also separated into the training set and part of the test set, in a proportion of 98:2, comprising 297,832 and 6079 samples, respectively. The detailed size of each dataset is described in the attachment.

Before inputting data into algorithms, it is common to use normalization to standardize data that are in different orders of magnitude. In this experiment, the data were preprocessed with standard normalization (standardscaler). Normalization can improve the convergence speed and model accuracy of neural networks. Because the normalization process is based on the training set, if the distribution state of the new data in the test set is different, the normalization will fail. In this process, temperatures from different positions in the FO-DTS were in a similar distribution state, i.e., the values did not vary widely. An AE and VAE were used; the number of epochs was 20 and the batch size was 64. Adam was used as the optimizer and the learning rate was set to 0.001. ReLU was used as the activation function. The details of the AE networks are shown in Table 2. For the loss function, the AE used MSE, and the VAE combined the reconstruction loss and the Kullback–Leibler divergence. The 95th percentile of the reconstruction errors from the training set was selected as the threshold for detections of anomalous temperatures. The test set consisted of 2% of the normal data and the entire data from the five anomalous scenarios, a total of 9634 samples.

##### 3.1.2. Anomaly Detection Performance Using Temporal Data

In the process of detection, if the algorithms fail to identify an anomaly, the missed detection is marked as false negative (FN), while classifying a normal event as an anomaly is marked as a false positive (FP). Specifically, to compare the anomaly detection performance across models, the delays in detecting temperature anomalies delays were collected.

**Table 2.** The brief structure of the (a) AE and (b) VAE model.

(a)		
Type	Layer	Description
Encoder	(0) Linear	in-features = 10, out-features = 128
	(1) ReLU	activation function
	(2) BatchNorm1d	in-features = 128, out-features = 128
	(3) Dropout	activation function
	(4) Linear	in-features = 128, out-features = 256
	(5) ReLU	activation function
	(6) BatchNorm1d	in-features = 256, out-features = 256
	(7) Dropout	$p = 0.2$
	(8) Linear	in-features = 256, out-features = 64
Decoder	(0) Linear	in-features = 64, out-features = 256
	(1) ReLU	activation function
	(2) BatchNorm1d	in-features = 256, out-features = 256
	(3) Dropout	$p = 0.2$
	(4) Linear	in-features = 256, out-features = 128
	(5) ReLU	activation function
	(6) BatchNorm1d	in-features = 128, out-features = 128
	(7) Dropout	$p = 0.2$
	(8) Linear	in-features = 128, out-features = 10
(b)		
Type	Layer	Description
Encoder	(dense1) Linear	in-features = 10, out-features = 128
	(dense2) Linear	in-features = 128, out-features = 256
	(dense3_mu) Linear	in-features = 256, out-features = 64
	(dense3_logvar) Linear	in-features = 256, out-features = 64
Decoder	(dense4) Linear	in-features = 64, out-features = 256
	(batch_norm) BatchNorm1d	in-features = 256, out-features = 256
	(dropout) Dropout	$p = 0.2$
	(dense5) Linear	in-features = 256, out-features = 128
	(recon) Linear	in-features = 128, out-features = 10

The overall performance of the algorithm ignoring the scenarios and the delay time of the algorithm's detection rate under different scenarios are shown in Table 3. The VAE significantly outperformed the AE in terms of recognition rate, with a recognition rate of 91.87%. In terms of detection latency, VAE also showed better performance in most scenarios, especially in Scenario 2 and Scenario 3, where the detection latency was 39 and 30 s, respectively, while the AE returned FNs in several scenarios. Unlike a standard AE, a VAE is inherently robust to noise and less prone to overfitting due to its use of variational inference and the reparameterization trick. This makes it better suited to handling variability in data compared with a basic autoencoder. Although these advantages mean that the VAE model can play an important role in data generation and the detection of temperature anomalies, if the normal and the anomalous data are similar enough or some other factors make the anomaly appear like a normal condition, the VAE cannot provide the expected results, e.g., relatively long detection delays were observed in Scenarios 1, 4, and 5.

**Table 3.** Results of temperature anomaly detection by the AE and VAE from a temporal perspective.

Model	Accuracy	Detection Delay (s)				
		Scene 1	Scene 2	Scene 3	Scene 4	Scene 5
AE	73.04%	FN	69	FN	FN	FN
VAE	91.87%	102	39	30	93	150

In order to compare different experimental scenarios, the ambient temperatures one hour before and after the experiment are shown in Figure 5a. At the beginning of heating, Scenario 2 and Scenario 3 both represented the hottest environment, but the ambient temperature of Scene 2 increased slowly, which did not have much effect on the anomalous temperature detection. Scenarios 1 and 3 included a decreasing trend in temperature, but the decreasing trend in Scenario 1 was relatively intense, so the delay in Scenario 1 was significantly higher than that in Scenario 3. At the beginning of heating, Scenario 3 and Scenario 2 both represented the hottest environment, but the ambient temperature in Scenario 3 was decreasing all the time. As shown in Figure 5b, although the temperature returned by the FO-DTS increased after heating, before the experiment, the temperature dropped dramatically with the environment.

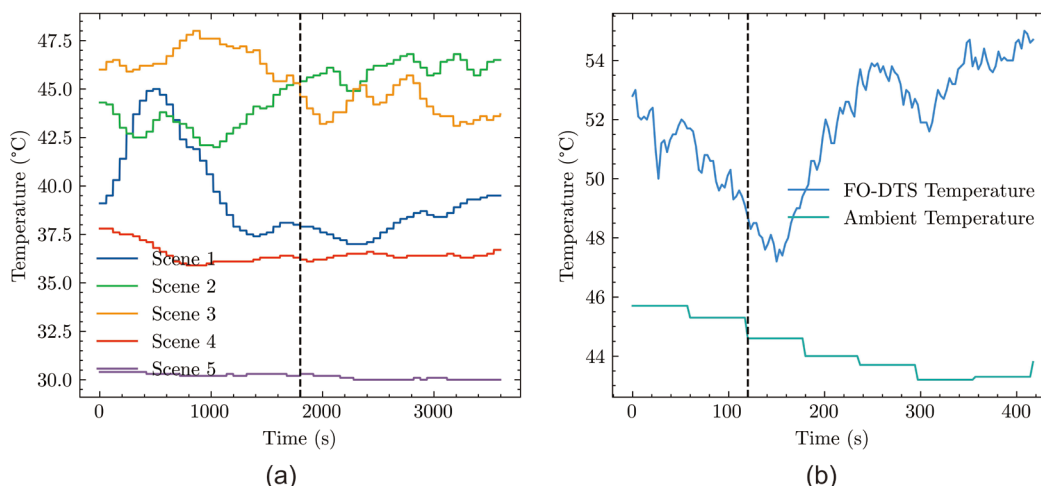


**Figure 5.** (a) Ambient temperature of different scenarios, (b) Ambient temperature for Scenario 3 and temperature from FO-DTS. Dashed line marks the start time of heating.

### 3.2. Detection of Temperature Anomalies Detection from a Spatial Perspective

#### 3.2.1. Spatial Model Design and Setting

In the spatial aspect, measurements from points along the whole monitoring path of the FO-DTS were taken to obtain the temperature data. Each ID represented different spatial locations of temperature measurement points at the same moment, and each ID corresponds to 10 temperature point featured in this study.

Before training the algorithms, spatial data were processed via standard normalization as described in Section 3.1.1. The algorithms were AE and VAE; ReLU was used as the activation function. The number of epochs was 20 and the batch size was 64. Adam was used as the optimizer and the learning rate was set to 0.001. Network details were the same as stated in Section 3.1.1. The loss function for AE was MSE, and VAE used a combination of reconstruction loss and the Kullback–Leibler divergence. A total of 303,983 data samples were obtained after division of the normal data. All the normal data were also separated into the training set and part of the test set, in a proportion of 98:2, comprising 297,903 and 6080 samples, respectively. The test set consisted of 2% of the normal data and the entire data from the five anomalous scenarios, a total of 9680 samples.

### 3.2.2. Anomaly Detection Performance Using Spatial Data

In the experiment, the anomaly detection threshold was determined using the 95th percentile of the reconstruction errors from the training set to assess the accuracy of the test set. This ensured that all algorithms were evaluated at the same level for anomalous temperature detection performance. As shown in Table 4, The overall recognition rate of VAE was 91.14%, which was slightly lower than the 92.58% achieved by the AE, but the difference was not significant. Although the overall recognition rate of the VAE was slightly lower than that of the AE, its detection speed was significantly faster than that of the AE model. The AE model had FNs in several scenarios, while the VAE model did not have FNs in any of the five scenarios, showing its higher stability.

**Table 4.** Results of temperature anomaly detection by the AE and VAE from a spatial perspective.

Model	Accuracy	Detection Delay (s)				
		Scene 1	Scene 2	Scene 3	Scene 4	Scene 5
AE	92.58%	FN	234	FN	FN	FN
VAE	91.14%	12	186	3	9	81

Generally, all of the rest had false negatives except Scenario 2, while Scenario 2 had the comparatively longest delay in detecting temperature anomalies. Various scenarios appeared to affect the likelihood of false negatives in detection of anomalous temperatures. As discussed in Section 2.2, from the spatial perspective, the AE was trained to recognize the characteristics of normal data that the temperature would keep consistent over a small range, and if the temperature had fluctuations in different positions, an anomaly event might happen. Since the VAE performed better in the spatial dimension, in order to understand the characteristics of the false positive samples in this test, we conducted an analysis to study the error distribution of the ten measurement points in the spatial dimension. Figure 6 shows that the variance of the measurement points in the central positions was relatively large.

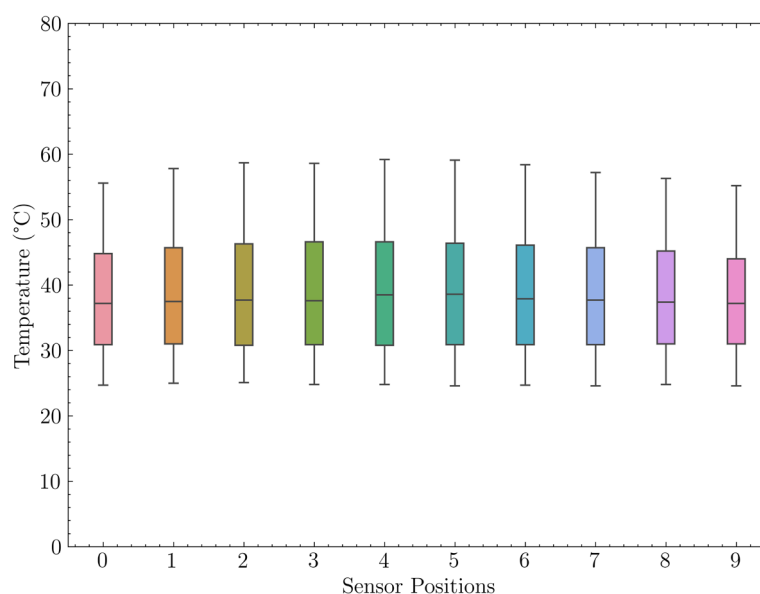


**Figure 6.** Box plots of VAE-based false positive samples from a spatial perspective.

### 3.3. Temperature Anomaly Detection from a Spatiotemporal Perspective

#### 3.3.1. Spatiotemporal Model Design and Setting

It is difficult to find an algorithm that performs well across all five scenes from a single perspective. Considering that the FO-DTS is a spatiotemporal measurement sensor, combining both spatial and temporal information may be a better approach. In this spatiotemporal dimension experiment, a 10 by 10 2D window was constructed, which represented a sliding window of 10 consecutive timestamps. At each timestamp, there were temperature values from 10 different measurement points, and each column represented the temperature variation at a specific measurement point across multiple timestamps.

Unlike the algorithms mentioned above, which process only one-dimensional data, handling two-dimensional inputs requires additional techniques. CNNs are inherently designed to work with multi-dimensional data, particularly images. Therefore, CNN-AE, which incorporates convolutional layers, can directly process spatiotemporal inputs. In contrast, traditional autoencoders, which use linear layers for computation, can only process data in one-dimension at a time. This study employed CNN-AE to handle two-dimensional inputs. CNN-AE is widely used; the kernel sizes in its convolutional layers are represented as two-dimensional arrays.

Datasets were reconstructed and for each input, the spatial dimensions were 10 and the temporal dimensions were 10. A total of 303,911 samples were obtained after division of the normal data. All the normal data were also separated into the training set and part of the test set, in a proportion of 98:2, including 297,832 and 6079 samples, respectively. As described in Sections 3.1.1 and 3.2.1, data were processed by standard normalization. The number of epochs was 20 and the batch size was 32. Adam was used as the optimizer and the learning rate was set to 0.001. MSE was set as the loss function and ReLU was used as the activation function. The details of the networks are shown in Table 5. The threshold for detection of temperature anomalies was set as the 97th percentile of the training set's loss value. The test set consisted of 2% of the normal data and the entire data from the five anomalous scenarios, a total of 9634 samples.

**Table 5.** Brief structure of the proposed CNN-AE model.

Type	Layer	Description
Encoder	(0) Conv2d	1, 64, kernel size = (3, 3), stride = (1, 1), padding = (1, 1)
	(1) ReLU	activation function
	(2) Conv2d	64, 128, kernel size = (3, 3), stride = (1, 1), padding = (1, 1)
	(3) ReLU	activation function
	(4) MaxPool2d	kernel size = 2, stride = 2, padding = 0, dilation = 1
Decoder	(0) ConvTranspose2d	128, 64, kernel size = (2, 2), stride = (2, 2)
	(1) ReLU	activation function
	(2) ConvTranspose2d	64, 1, kernel size = (3, 3), stride = (1, 1), padding = (1, 1)

#### 3.3.2. Anomaly Detection Performance Using Spatiotemporal Data

The convolutional layers of the CNN-AE effectively extract spatial features, and its recurrent structure can capture dynamic changes in time series. This combination of spatial and temporal features makes the CNN-AE more robust to environmental disturbances; the model achieved high detection rates across all five scenarios. As shown in Table 6, the average accuracy of the CNN-AE was 85.08%, with relatively stable performance across different scenes. Particularly in Scenarios 1 to 4, the CNN-AE demonstrated high detection

rates, showing good adaptability to different environmental conditions. Moreover, the CNN-AE exhibited consistent detection latency across these four scenarios, reflecting good temporal stability. Although the detection latency in Scenario 5 was slightly longer, the CNN-AE still maintained relatively low latency compared with the other models, especially under complex environmental conditions.

**Table 6.** Results of temperature anomaly detection by the CNN-AE from a spatiotemporal perspective.

Model	Accuracy	Detection Delay (s)				
		Scene 1	Scene 2	Scene 3	Scene 4	Scene 5
CNN-AE	85.08%	60	60	48	75	108

The determination of anomalies depends on the comparison between the reconstructed loss and the threshold, and the results of the reconstruction error over time for the five different scenes are shown in Figure 7 for further analysis. Overall, CNN-AE demonstrated robust performance across all scenes, effectively identifying anomalies and quickly returning to normal levels after an anomaly occurred.

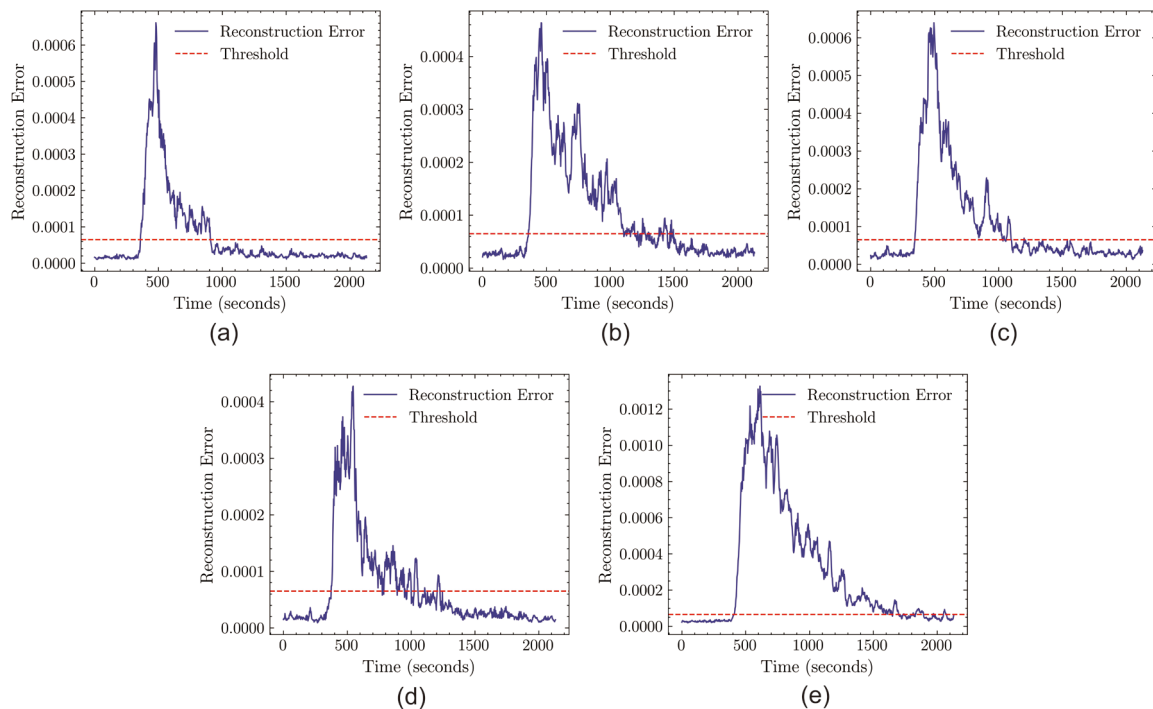


**Figure 7.** CNN-AE for spatiotemporal data anomaly detection: (a) Scenario 1 reconstruction error; (b) Scenario 2 reconstruction error; (c) Scenario 3 reconstruction error; (d) Scenario 4 reconstruction error; (e) Scenario 5 reconstruction error.

### 3.4. Discussion

Currently, research on AE-based fire detection revolves around how to exploit the properties of AE to improve the performance of fire warning systems. These studies involve feature extraction and dimensionality reduction, anomaly detection, multimodal data fusion, and real-time and computational resource optimization. Researchers have fused data from different types of sensors and employed AE for comprehensive analysis to further enhance the accuracy and reliability of fire detection [36,37,43]. However, these approaches also face some challenges; for complex data distributions, more complex network structures may be required to learn features effectively; training data may lead to false predictions if they do not adequately cover all normal operating conditions; handling

multimodal data increases the complexity of the system and requires solving the problems of data synchronization and calibration and, while pursuing a fast response, a certain degree of accuracy to improve the adaptability, accuracy, and response speed of the system in different environments.

Compared with the existing studies, this paper puts more emphasis on the influence of environmental factors on fire detection and explores the detection performance of different AE models. Meanwhile, this paper not only considers the changes in time series and spatial dimensions, but also integrates the spatiotemporal data of FO-DTS to construct a more comprehensive dataset, which helps to more accurately capture the characteristics of the fire occurrence and improve the adaptability and detection accuracy of the system.

Despite demonstrating the potential for detection of temperature anomalies using an FO-DTS and an AE, this study emphasizes that these methods should extend beyond theoretical exploration to support practical engineering applications. For deep learning methods, datasets are always the foundation of the algorithms. As presented in this study, after the installation of the FO-DTS, the temperature data returned from the sensor can serve as the training set for the algorithms. Theoretically, to mitigate algorithmic bias, it is advisable to collect data under varied conditions to ensure a balanced representation across different scenarios. Specifically, when constructing the dataset for the monitored equipment, temperature data should be collected in different weather conditions and at various times of the day, as abnormal increases in temperature can occur under any conditions, and the algorithms should learn patterns from all possible scenarios. Temperature trends can differ across seasons, and our study only considered summer conditions. We recommend preparing different datasets for each season so that the algorithms can focus more on the temperature characteristics relevant to the current time. Additionally, the datasets can be incrementally updated, allowing the algorithms to be retrained regularly to capture new patterns.

Determining the size of the input remains a challenge as the optimal parameters vary across different devices and scenarios, necessitating further research. In the context of the scenes discussed in this study, the spatial size of the input should at least be larger than the spatial resolution, and a temporal size greater than 60 would be preferable. If the spatial size of the input is smaller than the spatial resolution of the FO-DTS, it cannot provide accurate information about the spatial distribution of temperature, as spatial resolution represents the minimum length necessary for the FO-DTS to differentiate temperature measurements. Additionally, we suggest that the spatial size of the input should not be excessively large, as this can complicate spatial positioning. Regarding the temporal size, short time series are susceptible to random error interference and are unable to reflect accurately changes over time. Therefore, we recommend a larger temporal size to effectively reveal trends in temperature.

When the algorithm starts running, it serves as part of an outdoor fire alarm system to ensure the safety of life and property. Once the system reports an anomaly, it can coordinate and initiate appropriate emergency measures. Through these efforts, personnel can fully utilize the information provided by the FO-DTS to connect this spatiotemporal sensor with the fire alarm system. With the help of deep learning methods, reducing the rate of false alarms will enhance personnel's trust in the system, helping to avoid fatigue caused by excessive alerts.

#### 4. Conclusions

This study presents an enhanced method based on FO-DTS and autoencoders to address the challenges of poor performance of traditional data-driven models in outdoor fire warning, which are susceptible to environmental factors leading to false and missing

alarms in fire warning systems. An experimental setup with an electrical heating platform was constructed to simulate abnormal temperature rises, and the performance of various types of autoencoders, including AE, VAE, and CNN-AE, was tested. The results indicate that CNN-AE, which uses spatiotemporal data, offers superior detection rates and robustness, maintaining stable performance in complex environments. Although AE and VAE demonstrate slightly higher overall accuracy in some cases when using temporal or spatial dimensions, they exhibit lower performance in detection delay and anomaly detection rate, both of which are critical indices in anomaly detection for outdoor early fire warning. Environmental conditions such as temperature, humidity, and weather significantly impact detection results, with false alarms more likely to occur under high ambient temperatures and rapid temperature fluctuations.

Future research will focus on expanding datasets that incorporate diverse environmental factors to enhance the model's generalization capability and effectively evaluate the algorithm's performance across various scenarios. Additionally, the study will aim to further optimize the CNN-AE architecture to improve its accuracy and robustness in practical applications. Furthermore, integrating measurement data with environmental information and developing a model for the comprehensive detection of anomalies in complex scenarios could be considered.

**Supplementary Materials:** The following supporting information can be downloaded at: <https://www.mdpi.com/article/10.3390/fire8010023/s1>.

**Author Contributions:** Conceptualization, H.B. and X.Z.; Formal analysis, X.L. and Z.Z.; Investigation, X.L., Z.Z. and H.B.; Methodology, H.B. and X.Z.; Project administration, H.B.; Software, X.L., Z.Z. and Y.T.; Supervision, X.Z.; Validation, X.L. and X.Z.; Visualization, X.L., Z.Z. and Y.T.; Writing—original draft, H.B., X.L. and Z.Z.; Writing—review and editing, H.B. and X.Z. All authors have read and agreed to the published version of the manuscript.

**Funding:** This research was funded by the National Natural Science Foundation of China (No. 52004134) and the Postgraduate Research and Practice Innovation Program of Jiangsu Province 2024 (No. SJCX24\_0528).

**Data Availability Statement:** The original contributions presented in this study are included in the article/Supplementary Materials. Further inquiries can be directed to the corresponding author.

**Conflicts of Interest:** The authors declare no conflicts of interest.

## References

1. Meacham, B.J. Fire safety of existing residential buildings: Building regulatory system gaps and needs. *Fire Saf. J.* **2023**, *140*, 103902. [[CrossRef](#)]
2. Xie, D.; Chen, Q.; Zhu, Y. Optimal layout scheme of fire detectors and operation condition monitoring technology in urban integrated substation. *Measurement* **2024**, *236*, 115093. [[CrossRef](#)]
3. Hu, T.; Xu, Z.; Yu, C.; Dou, X.; Zhang, Y.; Sun, L. Impacts of different forest fire management policies and fuel treatment models on forest fire risk in boreal forest of China. *Ecol. Indic.* **2024**, *169*, 112806. [[CrossRef](#)]
4. Desai, A.; Heilman, W.E.; Skowronski, N.S.; Clark, K.L.; Gallagher, M.R.; Clements, C.B.; Banerjee, T. Features of turbulence during wildland fires in forested and grassland environments. *Agric. For. Meteorol.* **2023**, *338*, 109501. [[CrossRef](#)]
5. Wu, Y.; Sun, J.; Yang, G.; Cui, L.; Wang, Z.; Wang, M. Research on digital twin based temperature field monitoring system for LNG storage tanks. *Measurement* **2023**, *215*, 112864. [[CrossRef](#)]
6. Zhao, S.; Duan, Y.; Roy, N.; Zhang, B. A deep learning methodology based on adaptive multiscale CNN and enhanced highway LSTM for industrial process fault diagnosis. *Reliab. Eng. Syst. Saf.* **2024**, *249*, 110208. [[CrossRef](#)]
7. Linn, R.R.; Reisner, J.M.; Colman, J.; Winterkamp, J. Studying wildfire behavior using FIRETEC. *Int. J. Wildland Fire* **2002**, *11*, 233–246. [[CrossRef](#)]
8. Himoto, K.; Tanaka, T. Development and validation of a physics-based urban fire spread model. *Fire Saf. J.* **2008**, *43*, 477–494. [[CrossRef](#)]

9. Zhang, Q.; Zhu, J.; Dong, Y.; Zhao, E.; Song, M.; Yuan, Q. 10-minute forest early wildfire detection: Fusing multi-type and multi-source information via recursive transformer. *Neurocomputing* **2025**, *616*, 128963. [[CrossRef](#)]
10. Moritz, M.A.; Batllori, E.; Bradstock, R.A.; Gill, A.M.; Handmer, J.; Hessburg, P.F.; Leonard, J.; McCaffrey, S.; Odion, D.C.; Schoennagel, T.; et al. Learning to coexist with wildfire. *Nature* **2014**, *515*, 58–66. [[CrossRef](#)]
11. Luo, Y.-x.; Li, Q.; Jiang, L.-r.; Zhou, Y.-h. Analysis of Chinese fire statistics during the period 1997–2017. *Fire Saf. J.* **2021**, *125*, 103400. [[CrossRef](#)]
12. Yoshioka, H.; Himoto, K.; Kagiya, K. Large Urban Fires in Japan: History and Management. *Fire Technol.* **2020**, *56*, 1885–1901. [[CrossRef](#)]
13. Chowdhury, E.H.; Hassan, Q.K. Operational perspective of remote sensing-based forest fire danger forecasting systems. *ISPRS J. Photogramm. Remote Sens.* **2015**, *104*, 224–236. [[CrossRef](#)]
14. Amiro, B.D.; Cantin, A.; Flannigan, M.D.; de Groot, W.J. Future emissions from Canadian boreal forest fires. *Can. J. For. Res.* **2009**, *39*, 383–395. [[CrossRef](#)]
15. Prasad, D.; Nath, V. An Overview of Temperature Sensors. In *Proceeding of the Second International Conference on Microelectronics, Computing & Communication Systems (MCCS 2017)*; Nath, V., Mandal, J.K., Eds.; Springer: Singapore, 2019; pp. 777–784.
16. Wang, H.; Bah, M.J.; Hammad, M. Progress in Outlier Detection Techniques: A Survey. *IEEE Access* **2019**, *7*, 107964–108000. [[CrossRef](#)]
17. Chatterjee, P.; Kadir, S.U.; Srivastava, A.; Laszka, A. Chapter Seventeen—Grid resilience against wildfire with machine learning: Machine learning based detection, localization and mitigation of the impact of forest fires on power grids. In *Big Data Application in Power Systems*, 2nd ed.; Arghandeh, R., Zhou, Y., Eds.; Elsevier Science: Amsterdam, The Netherlands, 2024; pp. 393–417.
18. Ji, W.; Li, G.-Q.; Zhu, S.; Li, J.; Qi, H.; Wang, Y. Machine learning-driven real-time identification of large-space building fires and forecast of temperature development. *Expert Syst. Appl.* **2024**, *255*, 124758. [[CrossRef](#)]
19. Pang, G.; Shen, C.; Cao, L.; Hengel, A.V.D. Deep Learning for Anomaly Detection: A Review. *ACM Comput. Surv.* **2021**, *54*, 38. [[CrossRef](#)]
20. Chen, Y.; Morton, D.C.; Randerson, J.T. Remote sensing for wildfire monitoring: Insights into burned area, emissions, and fire dynamics. *One Earth* **2024**, *7*, 1022–1028. [[CrossRef](#)]
21. Toledo-Jaime, C.; Díaz-Avalos, C.; Chaudhuri, S.; Serra, L.; Juan, P. Understanding wildfire occurrence and size in Jalisco, Mexico: A spatio-temporal analysis. *For. Ecol. Manag.* **2024**, *573*, 122349. [[CrossRef](#)]
22. Toullier, T.; Dumoulin, J. Bias and bottlenecks study in outdoor long term thermal monitoring by infrared thermography: Leveraging opportunistic data for temperature estimation. *Infrared Phys. Technol.* **2024**, *141*, 105471. [[CrossRef](#)]
23. Dastour, H.; Ahmed, M.R.; Hassan, Q.K. Analysis of forest fire patterns and their relationship with climate variables in Alberta's natural subregions. *Ecol. Inform.* **2024**, *80*, 102531. [[CrossRef](#)]
24. Carrasco-Escaff, T.; Garreaud, R.; Bozkurt, D.; Jacques-Coper, M.; Pauchard, A. The key role of extreme weather and climate change in the occurrence of exceptional fire seasons in south-central Chile. *Weather Clim. Extrem.* **2024**, *45*, 100716. [[CrossRef](#)]
25. Junior, O.S.; Coninck, J.C.P.; Magrin, F.G.S.; Ganacim, F.I.S.; Pombeiro, A.; Fernandes, L.G.; Romanelli, E.F.R. Impacts of Atmospheric and Load Conditions on the Power Substation Equipment Temperature Model. *Energies* **2023**, *16*, 4295. [[CrossRef](#)]
26. Liu, S.-S.; Li, P.-W.; Lan, W.-h.; Lin, W.-j. High-temperature high-humidity and electrical static discharge stress effects on GaN p-i-n UV sensor. *Mater. Sci. Eng. B* **2005**, *121*, 29–33. [[CrossRef](#)]
27. Xing, H.; Fang, K.; Yao, Q.; Zhou, F.; Ou, T.; Liu, J.; Zhou, S.; Jiang, S.; Chen, Y.; Bai, M.; et al. Impacts of changes in climate extremes on wildfire occurrences in China. *Ecol. Indic.* **2023**, *157*, 111288. [[CrossRef](#)]
28. Diao, W.; Geng, Y. An Automatic Threshold Adjustment Algorithm for Thermal Fault Extraction. In *Proceedings of the 2023 6th International Conference on Software Engineering and Computer Science (CSECS)*, Chengdu, China, 22–24 December 2023; pp. 1–5.
29. Yang, S.; Huang, Q.; Yu, M. Advancements in remote sensing for active fire detection: A review of datasets and methods. *Sci. Total Environ.* **2024**, *943*, 173273. [[CrossRef](#)]
30. Saleh, A.; Zulkifley, M.A.; Harun, H.H.; Gaudreault, F.; Davison, I.; Spraggon, M. Forest fire surveillance systems: A review of deep learning methods. *Heliyon* **2024**, *10*, e23127. [[CrossRef](#)]
31. Gasser, J.; Warpelin, D.; Bussi eres, F.; Extermann, J.; Pomarico, E. Distributed temperature sensor combining centimeter resolution with hundreds of meters sensing range. *Opt. Express* **2022**, *30*, 6768–6777. [[CrossRef](#)]
32. Bao, Y.; Huang, Y.; Hoehler, M.S.; Chen, G. Review of Fiber Optic Sensors for Structural Fire Engineering. *Sensors* **2019**, *19*, 877. [[CrossRef](#)]
33. Neloy, A.A.; Turgeon, M. A comprehensive study of auto-encoders for anomaly detection: Efficiency and trade-offs. *Mach. Learn. Appl.* **2024**, *17*, 100572. [[CrossRef](#)]
34. Li, P.; Pei, Y.; Li, J. A comprehensive survey on design and application of autoencoder in deep learning. *Appl. Soft Comput.* **2023**, *138*, 110176. [[CrossRef](#)]
35. Bank, D.; Koenigstein, N.; Giryes, R. Autoencoders. *arXiv* **2020**, arXiv:2003.05991.

36. Xu, Z.; Guo, Y.; Saleh, J.H. Advances Toward the Next Generation Fire Detection: Deep LSTM Variational Autoencoder for Improved Sensitivity and Reliability. *IEEE Access* **2021**, *9*, 30636–30653. [[CrossRef](#)]
37. Üstek, İ.; Arana-Catania, M.; Farr, A.; Petrunin, I. Deep Autoencoders for Unsupervised Anomaly Detection in Wildfire Prediction. *Earth Space Sci.* **2024**, *11*, e2024EA003997. [[CrossRef](#)]
38. Qian, J.; Song, Z.; Yao, Y.; Zhu, Z.; Zhang, X. A review on autoencoder based representation learning for fault detection and diagnosis in industrial processes. *Chemom. Intell. Lab. Syst.* **2022**, *231*, 104711. [[CrossRef](#)]
39. Chu, C.; Zhu, Z.; Bian, H.; Jiang, J. Design of self-heating test platform for sulfide corrosion and oxidation based on Fuzzy PID temperature control system. *Meas. Control* **2021**, *54*, 1082–1096. [[CrossRef](#)]
40. Choi, K.; Yi, J.; Park, C.; Yoon, S. Deep Learning for Anomaly Detection in Time-Series Data: Review, Analysis, and Guidelines. *IEEE Access* **2021**, *9*, 120043–120065. [[CrossRef](#)]
41. He, H.; Garcia, E.A. Learning from Imbalanced Data. *IEEE Trans. Knowl. Data Eng.* **2009**, *21*, 1263–1284. [[CrossRef](#)]
42. Malhotra, P.; Ramakrishnan, A.; Anand, G.; Vig, L.; Agarwal, P.; Shroff, G.M. LSTM-based Encoder-Decoder for Multi-sensor Anomaly Detection. *arXiv* **2016**, arXiv:1607.00148.
43. Khan, Z.A.; Hussain, T.; Ullah, F.U.M.; Gupta, S.K.; Lee, M.Y.; Baik, S.W. Randomly Initialized CNN with Densely Connected Stacked Autoencoder for Efficient Fire Detection. *Eng. Appl. Artif. Intell.* **2022**, *116*, 105403. [[CrossRef](#)]

**Disclaimer/Publisher’s Note:** The statements, opinions and data contained in all publications are solely those of the individual author(s) and contributor(s) and not of MDPI and/or the editor(s). MDPI and/or the editor(s) disclaim responsibility for any injury to people or property resulting from any ideas, methods, instructions or products referred to in the content.